Available online at www.sciencedirect.com
SCIENCE DIRECT®
Journal of Sound and Vibration 269 (2004) 569–588
JOURNAL OF SOUND AND VIBRATION
www.elsevier.com/locate/jsvi

Optimal design of PZT actuators in active structural acoustic control of a cylindrical shell with a floor partition

D.S. Li[a], L. Cheng[b,*], C.M. Gosselin[a]

[a] Department of Mechanical Engineering, Laval University, Que., Canada G1K 7P4,
[b] Department of Mechanical Engineering, The Hong Kong Polytechnic University, Hong Kong, China

Received 12 February 2002; accepted 13 January 2003

Abstract

Genetic algorithms (GAs) are employed to optimize locations of PZT actuators in an active structural acoustic control (ASAC) system comprising a cylindrical shell with an internal floor partition. The effect of PZT actuators is simulated using a bending model and an in-plane force model, respectively. The characteristics of the optimal placements of both models are discussed and compared. Numerical simulations demonstrate that for the investigated structure, the in-plane force model has a better control performance than the bending model in the low-frequency range. The underlying physics of the control results are analyzed. Considering the practical applicability of optimally designed ASAC systems, the control performance of the optimal configuration obtained at a single frequency is assessed in the low-frequency range between 100 and 500 Hz, with results showing a significant sound attenuation in the whole range of interest.
© 2003 Elsevier Science Ltd. All rights reserved.

1. Introduction

Due to the requirement of attenuating the interior low-frequency noise enclosed by vibrating structures, active control technology has been widely investigated in the literature in past decade. In an active noise control system, a secondary sound field is introduced either by acoustic sources (e.g., loudspeakers) or by vibration sources (e.g., piezoelectric actuators or mini-shakers) on the enclosing structure to cancel the primary sound field produced by the disturbance. The control performance depends on the extent of temporal and spatial match between the primary and secondary sound field. The temporal match is determined by an electronic control system. The

*Corresponding author. Fax: +852-2365-4703.
E-mail address: mmlcheng@polyu.edu.hk (L. Cheng).

0022-460X/03/$ - see front matter © 2003 Elsevier Science Ltd. All rights reserved.
doi:10.1016/S0022-460X(03)00044-0

spatial match, however, is mainly influenced by a spatial arrangement of both actuators and error sensors. Therefore, with the assumption that an electronic control system can perfectly execute the desired control action, the spatial configuration, that is, the placement of control sources and error sensors will be the key factors determining the effectiveness of a control system. Considering the high cost of active control experiment, the optimal design of the physical control system becomes essential to ensure the efficiency of an active noise control system before the system is implemented.

Different optimization approaches were employed in the design of active noise control systems. Using the conventional gradient-based optimization routines, Clark and Fuller [1] determined the size and the location of piezoelectric actuators and sensors on a rectangular plate for active structural acoustic control (ASAC). Although the method has the advantage of fast convergence, the search can be easily trapped to a local optimum for complex multi-modal problems such as the noise control in complex enclosures. An alternative is to use the exhaustive search in all possible configurations to determine the global optima. However, it is impractical for a large space search problem due to the high computation cost.

With the merits of robustness and high efficiency in dealing with the complex multi-model non-linear problems, Genetic algorithms (GAs) have been recognized as a promising optimization tool in the active noise and vibration control field by many researchers. Baek and Elliott [2] optimized the locations of loudspeakers in an active noise control systems using GAs and the Simulated Annealing Algorithm. Both methods showed good performance. However, compared with GAs, the performance of Simulated Annealing Algorithm is somewhat more sensitive to the parameters used in the algorithms. Simpson and Hansen [3] investigated the application of GAs in optimizing the placement of vibration control sources in ASAC system, in which the performance of simple GA and various improved GAs is compared, showing that the steady state genetic algorithm with multi-variable binary string coding, forced mutation, and sharing is the most efficient scheme for the investigated problem. Ratle and Berry [4] used the GAs to optimize the point-masses placement to reduce the sound radiation of a plate. Kim and Song [5] optimized the placement of PZT and the electrode shape of PVDF sensors by GAs to minimize the well-radiating modes identified in advance by the radiation efficiency analysis. Besides their applications in the location optimization, GAs were also used in structural design to make the structure a passive noise filter in a certain frequency band [6].

Although the past work reported in the literature has demonstrated the good performance of GAs in various applications, most of them dealt with the placement optimization of point actuators or the problems of sound radiation into free field from beams and plates. Because of the merits of lightweight and easy installation, PZT actuators are becoming a very attractive option of actuators in ASAC. Obviously, the control effect of PZT actuators is different from that of point forces. The fact that PZT actuators generate distributed effects to the structure over the covered area makes the problem of optimal placement design more critical.

In this paper, the location optimization of PZT actuators in an ASAC system of a cylindrical shell with an internal floor partition is investigated using GAs. The primary physical model was previously developed to simulate the sound field inside an aircraft cabin. The present work does not claim any contribution on GAs development. Instead, it focuses on the physical problem itself. In this paper, the load effect of PZT actuators is simulated using a bending model and an in-plane force model, respectively, instead of point forces. The characteristics of the optimal

placement of both PZT models are discussed. The control performances of both models are assessed and compared. The underlying physics of the optimal design results are analyzed. Considering the requirement of practical application of ASAC, the optimal configuration of the control system obtained at a single frequency is also tested in the low-frequency range between 100 Hz, below which there are no any structural and acoustic natural frequencies for the investigated structure, and 500 Hz. In terms of GAs, besides the coding scheme and selection mechanism, etc., parameters used in GAs could also significantly influence the search performance, and they are rather problem-dependent. To improve the search performance, the parameter values are firstly optimized before the GAs are used in the design.

2. Theoretical models and optimization approach

2.1. Structural and acoustic models

The structure to be considered in the present research consists of a thin finite circular cylindrical shell with a longitudinal floor partition as shown in Fig. 1. u_s, v_s, w_s are the longitudinal, tangential, and radial displacement of the shell and u_f, v_f, w_f the displacement of the floor in the x, y_f, z_f direction respectively. θ_f represents the position of the floor, θ is the circumferential coordinate of the shell and L the length of the shell. Both the shell and the floor are assumed to be homogeneous and isotropic. The boundary conditions of the shell–floor structure are considered simply supported at the two ends. As far as the acoustic boundary condition is concerned, the

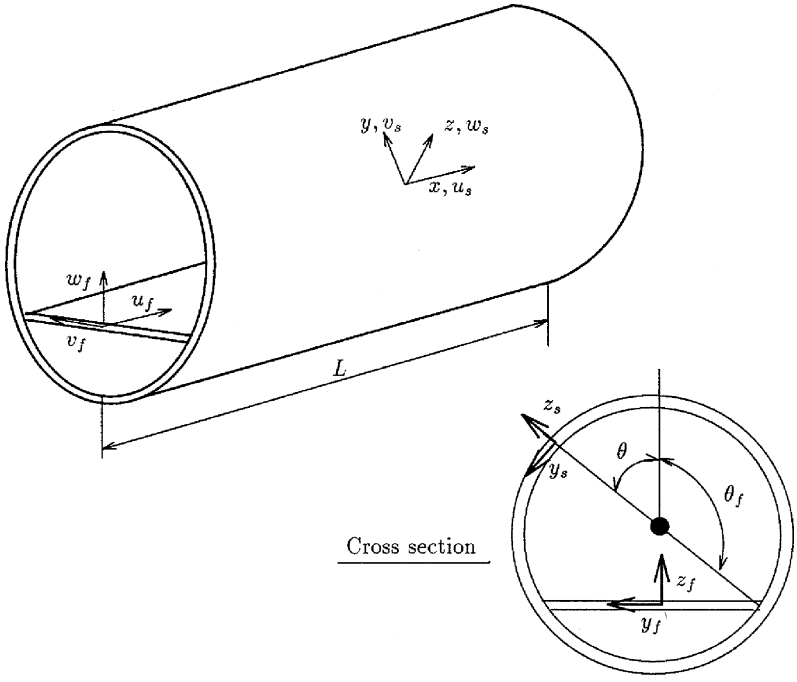

Fig. 1. The structure of a cylindrical shell with a floor partition.

shell wall and the floor are assumed to be flexible while the two end plates are assumed to be acoustically rigid.

The structural model is detailed in the previous work [7]. The Rayleigh–Ritz method is used to develop the structural model. The displacements of the shell in three directions (i.e., the longitudinal, circumferential and radial directions) are decomposed on the basis of the natural modes of a plain cylindrical shell. For the floor, both transverse and in-plane motions are expanded using the floor natural modes as trial functions. Structural coupling between the shell and the floor is simulated using an artificial spring system [8] for every permitted degree of freedom. The stiffness of all springs is assumed to uniformly distribute along the two shell-floor junctions.

The sound field is modelled using the Integro-Modal approach [9], which was developed for analyzing the acoustic properties of irregular cavities, where it is not possible to apply the technique of separation of variables. An irregularly shaped enclosure is handled as a multi-connected cavity system, with either regular or slightly irregular sub-volumes. A virtual membrane separates each pair of adjacent sub-cavities. An integral formulation ensures global continuity of the pressure between adjacent sub-cavities by assigning a zero-mass and zero-stiffness to the membrane. The cavity is discretized into N sub-cavities of both regular and irregular shapes. The Modal characteristics of regular sub-cavities are analytically available for performing sound pressure decomposition. For irregular sub-cavities, the modes of the bounding sub-cavities (called envelope), which are chosen to be of regular shape, are used to perform the pressure decomposition and to obtain the Green function.

2.2. Models of PZT actuators

Two analytical models of PZT actuators [10] (i.e., bending and in-plane force models), adapted from the models developed for plates [11,12], are employed here to simulate the effect of a pair of PZT actuators attached on the opposite sides of cylindrical shell wall. The bending model simulates the effect of two actuators operating out of phase, which produces an axial stress distribution varying linearly through the thickness of the cylinder wall and creates bending about the middle surface of the cylinder. The loading produced on the cylinder by the bending model is approximated by line moment distribution acting on the perimeter of the piezoelectric patch area (Fig. 2 (a)). According to the vibration theory of shells [13], the radial loading of the cylinder due to the line moment distribution can be expressed as

$$f_r(x,\theta) = \frac{\partial m_\theta}{\partial x} + \frac{1}{a}\frac{\partial m_x}{\partial \theta}, \tag{1}$$

where

$$m_x = CV[H(x-x_1) - H(x-x_2)][\delta(y-y_2) - \delta(y-y_1)], \tag{2}$$

$$m_\theta = CV[H(y-y_1) - H(y-y_2)][\delta(x-x_2) - \delta(x-x_1)] \tag{3}$$

and a is the radius of the cylindrical shell.

In Eqs. (2) and (3), C is a constant related to structural material properties, piezoelectric properties, and mechanical coupling parameters, V is the complex input voltage of actuators, $H(x)$ is the unit step function, $\delta(x)$ is the Dirac delta function, and $y = a\theta$.

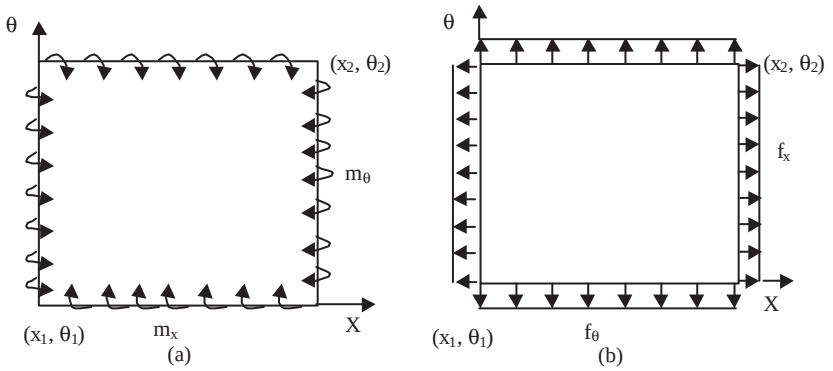

Fig. 2. Models of PZT actuators: (a) Bending model, (b) in-plane force model.

With the in-plane force model, the actuators are assumed to operate in-phase. When this model is implemented on a flat plate, only in-plane displacements are produced. In the case of a cylinder however, bending displacement is also induced by the in-plane deformation due to the curvature effects intrinsic to shells. Hence, it is possible to employ this model in the ASAC of a cylindrical structure. The in-plane loading can be simulated by a line force distribution on the perimeter of the patch area (Fig. 2 (b)), which can be expressed as follows

$$f_x = FV[H(y - y_1) - H(y - y_2)][\delta(x - x_2) - \delta(x - x_1)], \tag{4}$$

$$f_\theta = FV[H(x - x_1) - H(x - x_2)][\delta(y - y_2) - \delta(y - y_1)], \tag{5}$$

where F is a constant depending on the structural material properties, piezoelectric properties and mechanical coupling parameters.

It should be pointed out that because the models are adapted from flat plate theory, the curvature effect of the PZT patches is not taken into account. Therefore, these models are suitable only when the patch dimensions of PZT actuators are small relative to the cylinder radius so that the error caused by neglecting curvature effects in the actuator loading is negligible.

2.3. Optimization approach

Thanks to their strong search ability, GAs are used here to explore the location space of PZTs on the structure surface. Genetic algorithms [14,15] are stochastic search techniques based on the mechanism of natural selection and natural genetics. Differing from conventional search techniques, they start with an initial set of random solutions called population. The offspring is generated through a crossover operator and/or a mutation operator. Then, a smaller group of offspring are selected, according to the fitness values, to form a new generation. A conventional approach of selection is called roulette wheel method where each current individual in the population has a slot sized in proportion to its fitness. Hence, the individual with good fitness will have more chance to be selected for reproduction. After many generations, the algorithms converge to one individual, which very possibly represents the optimal or sub-optimal solution to the problem.

Genetic Algorithms such as the steady state genetic algorithm (SSGA), the selector of the stochastic remainder sampling (SRS) without replacement, the sharing scheme, and the binary coding scheme, which have been proven to be effective in Refs. [3,14,15], are directly used here as the research tool. The reduction of the acoustic potential energy in the enclosure is used as the evaluation criteria.

For each chromosome in GAs, i.e., each possible PZT actuator configuration, the control effort is determined using the quadratic optimization approach [16] by minimizing the acoustic potential energy in the enclosure defined as

$$E = \frac{1}{4\rho_0 c_0^2} \int_v |p(r)|^2 \, \mathrm{d}v, \tag{6}$$

where ρ_0, c_0 are the fluid density and the sound speed, respectively, r is the spatial co-ordinate of a point in the enclosure.

In Eq. (6), the sound pressure terms can be expanded as a sum of modal contributions

$$p(r) = \sum_{i=1}^{\infty} p_i \varphi_i(r), \tag{7}$$

where p_i and $\varphi_i(r)$ are the complex pressure amplitude and mode shape, respectively, of the ith acoustic mode. Substituting this expansion into Eq. (6) and using the orthogonal properties of the acoustic modes, one obtains

$$E = \frac{1}{4\rho_0 c_0^2} \sum_{i=1}^{\infty} \Lambda_i |p_i|^2, \tag{8}$$

where Λ_i is the volume normalization of the ith acoustic mode which is defined as

$$\Lambda_i = \int \varphi_i^2(r) \, \mathrm{d}r. \tag{9}$$

As a linear system is considered, the total acoustic pressure at any given location in the enclosure during operation of the active control will be equal to the sum of the primary and control components as

$$p(r) = p_c(r) + p_p(r), \tag{10}$$

where the subscripts p and c denote primary and control sources, respectively.

Combining Eqs. (8) and (10) and then using the modal coupling theory, one obtains the acoustic potential energy in enclosures

$$E = \mathbf{V}_c^H \mathbf{A} \mathbf{V}_c + \mathbf{V}_c^H \mathbf{b} + \mathbf{b}^H \mathbf{V}_c + \tilde{E}, \tag{11}$$

where $\mathbf{V}_c$ is the vector of the control input;

$$\mathbf{A} = \boldsymbol{\psi}_{gc}^{\mathrm{T}} \{\mathbf{Z}_I^{-1}\}^H \mathbf{B}^{\mathrm{T}} \mathbf{Z}_a^H \mathbf{Z}_E \mathbf{Z}_a \mathbf{B} \mathbf{Z}_I^{-1} \boldsymbol{\psi}_{gc}, \tag{12}$$

$$\mathbf{b} = \boldsymbol{\psi}_{gc}^{\mathrm{T}} \{\mathbf{Z}_I^{-1}\}^H \mathbf{B}^{\mathrm{T}} \mathbf{Z}_a^H \mathbf{Z}_E \mathbf{Z}_a \mathbf{B} \boldsymbol{\upsilon}_p \tag{13}$$

in which $\tilde{E}$ is the potential energy induced by the primary force calculated as

$$\tilde{E} = \mathbf{v}_p^H \mathbf{B}^{\mathrm{T}} \mathbf{Z}_a^H \mathbf{Z}_E \mathbf{Z}_a \mathbf{B} \mathbf{v}_p. \tag{14}$$

Then the vector of the optimum control input can be written as

$$\mathbf{V}_{c,E} = -\mathbf{A}^{-1}\mathbf{b}, \tag{15}$$

leading to a minimum value of acoustic potential energy equal to

$$E_{min} = \tilde{E} - \mathbf{b}^{H}\mathbf{A}^{-1}\mathbf{b}. \tag{16}$$

In the above equations, $\mathbf{Z}_a$ is the diagonal matrix containing acoustic modal radiation transfer functions; $\mathbf{Z}_E$ is the diagonal weighting matrix; $\mathbf{Z}_I$ is the structural modal input impedance matrix; $\mathbf{B}$ is the matrix of modal coupling coefficients between acoustic modes and structural modes; $\boldsymbol{\upsilon}_p$ is the vector of structural modal velocities resulting from the primary forces; $\boldsymbol{\psi}_{gc}$ is the matrix containing modal generalized force transfer functions and depends on the type of control sources. When PZT actuators are used, its component ψ_{ij} can be calculated by

$$\psi_{ij} = \int_s \phi_i(x,\theta) f_j(x,\theta)\, \mathrm{d}s, \tag{17}$$

where ψ_{ij} is the ith modal generalized force transfer function of jth actuator with loading distribution $f_j(x,\theta)$, and $\phi_i(x,\theta)$ is the modal shape of ith mode of the investigated structure.

The ith radial, longitudinal and tangential modal shapes of the cylindrical shell in the structural model can be respectively expressed as

$$\phi_i^r = \sum_{\alpha=0}^{1}\sum_{m=1}^{\infty}\sum_{n=0}^{\infty} c_{mn}^{\alpha}\cos\left(n\theta - \alpha\frac{\pi}{2}\right)\sin\left(\frac{m\pi x}{L}\right), \tag{18}$$

$$\phi_i^x = \sum_{\alpha=0}^{1}\sum_{m=1}^{\infty}\sum_{n=0}^{\infty} c_{mn}^{\alpha} a_{mn}\cos\left(n\theta - \alpha\frac{\pi}{2}\right)\cos\left(\frac{m\pi x}{L}\right), \tag{19}$$

$$\phi_i^{\theta} = \sum_{\alpha=0}^{1}\sum_{m=1}^{\infty}\sum_{n=0}^{\infty} c_{mn}^{\alpha} b_{mn}\sin\left(n\theta - \alpha\frac{\pi}{2}\right)\sin\left(\frac{m\pi x}{L}\right). \tag{20}$$

In Eqs. (18), (19), and (20), a_{mn} and b_{mn} is the modal vector of the corresponding simply supported shell with n and m being, respectively, the circumferential and longitudinal order; $\alpha = 0$ (or 1) means symmetric (or anti-symmetric) mode; c_{mn}^{α} are the coefficient determined by the free vibration analysis of the investigated structure with the inclusion of the floor [7]; and a is the radius of the shell.

It should be noted that since the effect of the mass and stiffness of PZT actuators on the structure is small, the mode shapes of the structure are assumed to be the same after PZT actuators are attached.

When the bending model is used, by substituting Eq. (1) with an unit actuator input voltage and Eq. (18) into Eq. (17), the ith circumferential modal generalized force transfer function can be

obtained as

$$\psi_{ij}^{r} = M \sum_{\alpha=0}^{1} \sum_{m=1}^{\infty} \sum_{n=0}^{\infty} c_{mn}^{\alpha} \begin{cases} \dfrac{m\pi a}{L}(\theta_2 - \theta_1) \cos\left(\alpha\dfrac{\pi}{2}\right)\left[\cos\left(\dfrac{m\pi x_1}{L}\right) - \cos\left(\dfrac{m\pi x_2}{L}\right)\right] & n = 0 \\ \left(\dfrac{m\pi a}{nL} + \dfrac{nL}{m\pi a}\right)\left[\sin\left(n\theta_2 - \alpha\dfrac{\pi}{2}\right) - \sin\left(n\theta_1 - \alpha\dfrac{\pi}{2}\right)\right] & \\ \times\left[\cos\left(\dfrac{m\pi x_1}{L}\right) - \cos\left(\dfrac{m\pi x_2}{L}\right)\right] & n \neq 0 \end{cases} \tag{21}$$

When PZT actuators are assumed to operate as an in-plane force model, by substituting Eq. (4) with unit actuator input voltage and Eq. (19) into Eq. (17), one obtains the ith longitudinal modal generalized force transfer function as follows:

$$\psi_{ij}^{x} = F \sum_{\alpha=0}^{1} \sum_{m=1}^{\infty} \sum_{n=0}^{\infty} c_{mn}^{\alpha} a_{mn} \begin{cases} a(\theta_2 - \theta_1) \cos\left(\alpha\dfrac{\pi}{2}\right)\left[\cos\left(\dfrac{m\pi x_2}{L}\right) - \cos\left(\dfrac{m\pi x_1}{L}\right)\right] & n = 0 \\ \dfrac{a}{n}\left[\sin\left(n\theta_2 - \alpha\dfrac{\pi}{2}\right) - \sin\left(n\theta_1 - \alpha\dfrac{\pi}{2}\right)\right] & \\ \times\left[\cos\left(\dfrac{m\pi x_2}{L}\right) - \cos\left(\dfrac{m\pi x_1}{L}\right)\right] & n \neq 0 \end{cases} \tag{22}$$

Substituting Eq. (5) with unit actuator input voltage and Eq. (20) into Eq. (17), one could get the ith tangential modal generalized force transfer function as

$$\psi_{ij}^{\theta} = F \sum_{\alpha=0}^{1} \sum_{m=1}^{\infty} \sum_{n=0}^{\infty} c_{mn}^{\alpha} b_{mn} \frac{L}{m\pi}\left[\sin\left(n\theta_2 - \alpha\frac{\pi}{2}\right) - \sin\left(n\theta_1 - \alpha\frac{\pi}{2}\right)\right] \times \left[\cos\left(\frac{m\pi x_1}{L}\right) - \cos\left(\frac{m\pi x_2}{L}\right)\right]. \tag{23}$$

Combining the GAs, the structural and acoustic models, the PZT actuator model, and the quadratic optimization approach together, the location optimization of PZT actuators can be performed. Some typical results are given in the following sections.

3. Numerical results and analysis

Numerical results presented hereafter use the following configuration: the shell and the floor are assumed to have the same thickness of 0.0032 m, the density of material 7860 kg/m^3, Poisson ratio 0.3, Young's modulus 2.07×10^{11} N/m^2, the length of the cylindrical shell 1.209 m, the radius 0.254 m, sound speed 343 m/s, air density 1.2 kg/m^3, and modal loss factor for the structure and the cavity 5×10^{-3}. The shell–floor attachment is assumed to be rigid. The position of the floor is defined by $\theta_f = 131^\circ$ (Fig. 1). Since the values of constants C and F (used in PZT models) do not affect the optimization results, they are assumed to be 1 in the calculation.

In the design reported hereafter, the disturbance is assumed to be point forces; and PZT actuators provide control actions. The size of each actuator is 0.05 m × 0.02 m covering a sector angle of 4°. To avoid that a control actuator is too close or even overlaps with a disturbance force, a clearance distance between a disturbance and a control actuator, which is 0.05 m in the longitudinal direction or 10° in the circumferential direction, is imposed. The overlap among control PZT actuators is avoided using the forced mutation method. The search space is the

positions on the shell surface with a resolution of 0.01 m in the longitudinal direction and 1° in the circumferential direction. It should also be pointed out that in the context, one PZT actuator refers to a pair of PZT actuators attached on the opposite side of the cylindrical shell wall.

3.1. Parametric study of genetic algorithms

A suitable choice of parameters used in GAs would significantly affect the optimization process. A thorough understanding and investigation of this issue is crucial to ensure the effectiveness and correctness of the results. This issue should be investigated on a case-by-case basis since it strongly depends on the problem and the structure under investigation. Hence, before the GAs are used in the design, these parameters are firstly studied using a simple case involving one primary point force and one control point force as a test example. On one hand, the computation time is short due to its simplicity; on the other hand, the results can be directly used in subsequent optimizations using the same physical structure. The structure is assumed to be excited at (0.31 m, 90°) by a point force of 1 N at 480 Hz. The average of the best of generation results of ten consecutive runs are compared.

The effect of the crossover probability P_c is firstly tested with the values 0.6, 0.8, and 1.0, respectively. The searching performance is shown in Fig. 3 in which the total acoustic potential energy reduction is expressed in dB against the number of generations. It can be seen that although the convergence speed with different P_c values is somehow quite different at the earlier stage of the generation, actually, only with the crossover probability 1.0, the search converges to the global optimum giving the maximum reduction. Due to the high ability of exploiting the information in the population as $P_c = 1.0$ and the reduced stochastic errors of sampling through the use of more accurate selection procedures such as SRS without replacement, the search is less likely to stagnate at a local optimum.

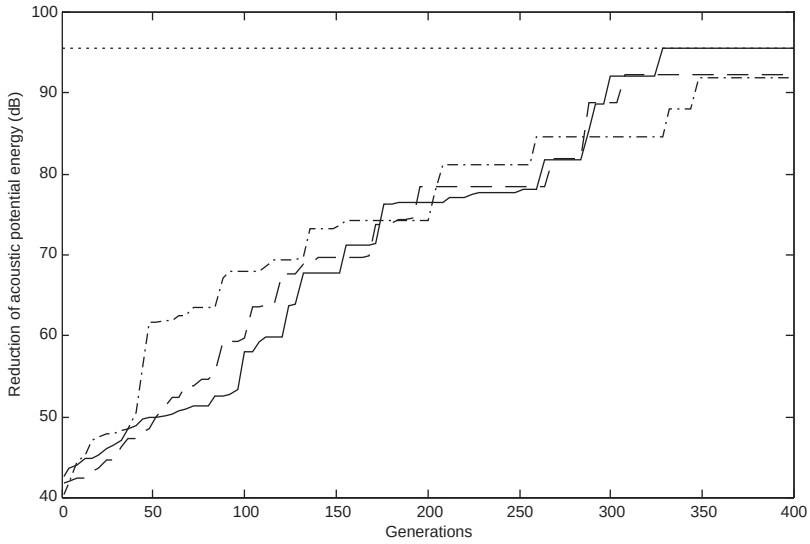

Fig. 3. Effect of crossover probability on search performance. · · · · ·: Maximum reduction, - - - - - -: $P_c = 0.6$, ------: $P_c = 0.8$, ——: $P_c = 1.0$.

The search behavior with different mutation rates (0.04, 0.06, and 0.08) is illustrated in Fig. 4. It is demonstrated that only in the case of the mutation rate $P_m = 0.06$, the search ends up with the global optimum in each run whilst the convergence percentage is 80% in the case of $P_m = 0.04$ and 50% when $P_m = 0.08$. With the mutation rate $P_m = 0.04$, the ability of exploring new information in the search procedure is reduced, which can easily cause the search to stagnate at a local optimum. On the contrary, with high mutation rate of $P_m = 0.08$, the search becomes more random and lacks focus on higher fitness individuals. This is consistent with De Jong's observation [17] showing that if $P_m = 0.1$, the search behavior will be the same as that of a random search. As a result, 0.06 will be used as the optimal value of the mutation rate in this work.

The effect of the population size P_s on the search performance is shown in Fig. 5 using respectively 50, 100, and 200. To make the comparison objective and fair to different population sizes, the number of search strings is kept constant for each case (40,000). From Fig. 5, one can observe that within the same number of search strings, the search with population size 100 converges to the global optimum at each run. The convergence probability to the global optimum is only 60% for the population size 50 and 70% for the population size 200. The possible reason is that as the population size is too small, the probability for offspring to get new genes through crossover and mutation is low, hence, the diversity of the population is limited and the search is much easier to be trapped at a local optimum. When the population of a species is too big however, the offspring could be so diverse that it makes the evolution difficult to converge to a global optimum within a certain number of search strings due to the lack of focus on higher fitness individuals.

As a result of the parametric study, the following parameter values will be used in the following optimization problem: $P_c = 1.0$, $P_m = 0.06$, and $P_s = 100$. These relatively optimal parameter values together with the use of the advanced techniques of GAs will certainly help the search converge to a global optimum instead of local ones.

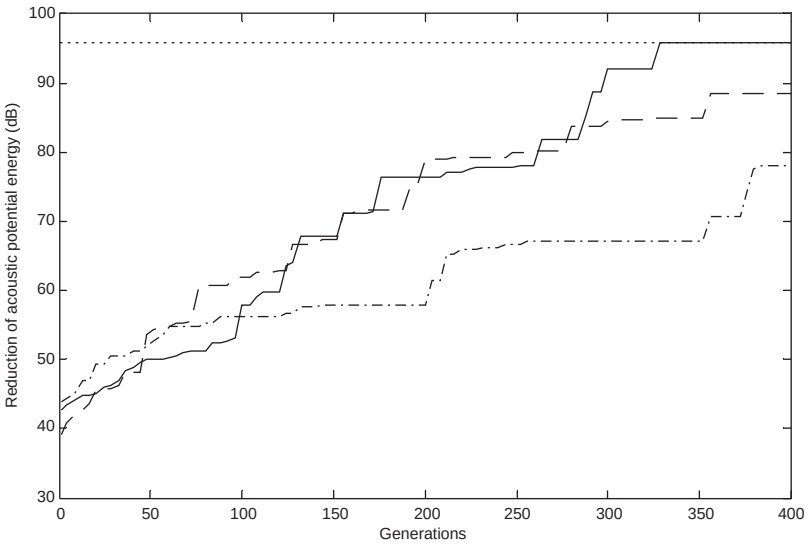

Fig. 4. Effect of mutation rate on search performance. · · · · ·: Maximum reduction, - - - - -: $P_m = 0.04$, ——: $P_m = 0.06$, - · - · - · -: $P_m = 0.08$.

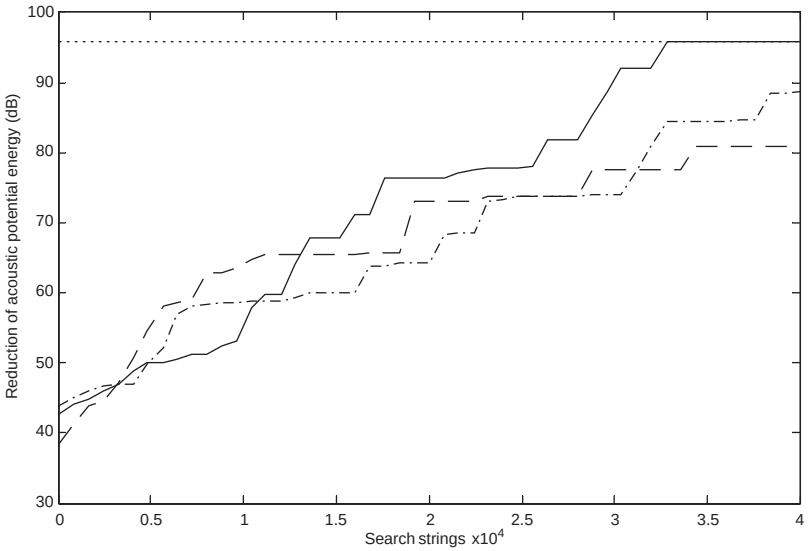

Fig. 5. Effect of population size on search performance. · · · · ·: Maximum reduction, - - - - -: $P_s = 50$, ——: $P_s = 100$, - · - · - · -: $P_s = 200$.

3.2. Placement optimization of PZT actuators operating as a bending model

In this section, the optimal location and the control performance are discussed while PZT actuators operate as a bending model. First, a simple case of one primary force and one PZT actuator is investigated. It is assumed that the shell–floor structure is excited by a 1 N point force locating at (0.31 m, 90°) on the shell surface. The design was carried out at an acoustic resonant frequency of 283.7 Hz. The optimal configuration is shown in Fig. 6, in which the shell surface is cut along the longitudinal direction at $\theta = 0°$ and stretched into a plane surface. Also in the figure, the small square represents the location of the disturbance whilst the rectangular strip gives the optimal PZT location. The optimal position of the PZT actuator is (0.62 m, 85°), which, contrary to what people might think, is not very close to the disturbance either in the circumferential or in the longitudinal direction. At the design frequency, a sound reduction of 37.0 dB is achieved. In order to interpret the control result, the squared velocity response spectra of structural modes before and after the control are shown in Fig. 7. In this figure, the dotted and solid lines represent the cases before and after control respectively. Since there are no natural modes below 100 Hz, the frequency range shown in the figure starts from 100 Hz. It can be observed that before control, the structural modes at 267.8 and 290.5 Hz are predominant in the structural vibration. The structural coupling analysis using the radiation efficiency analysis of structural modes (REASM) method [18] also shows the high radiation efficiency of these two modes. Therefore, to achieve a significant noise reduction, the PZT actuator should effectively suppress these two modes. This is confirmed by investigating the modal response after the control is applied. As shown in Fig. 7, the responses of these two modes are indeed considerably attenuated. This result suggests that the optimally designed PZT actuator can effectively suppress the structural modes significantly radiating sound into the enclosure.

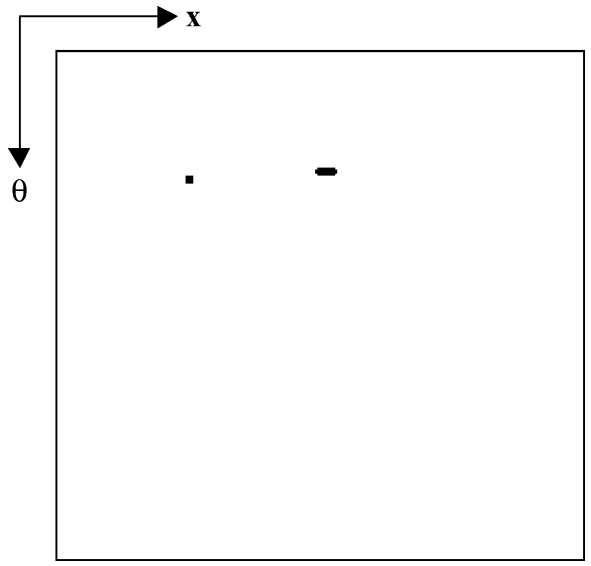

Fig. 6. Optimal placement of PZT actuators operating as a bending model in the case of one primary force and one control actuator. ■: Disturbance, ▬: PZT actuator.

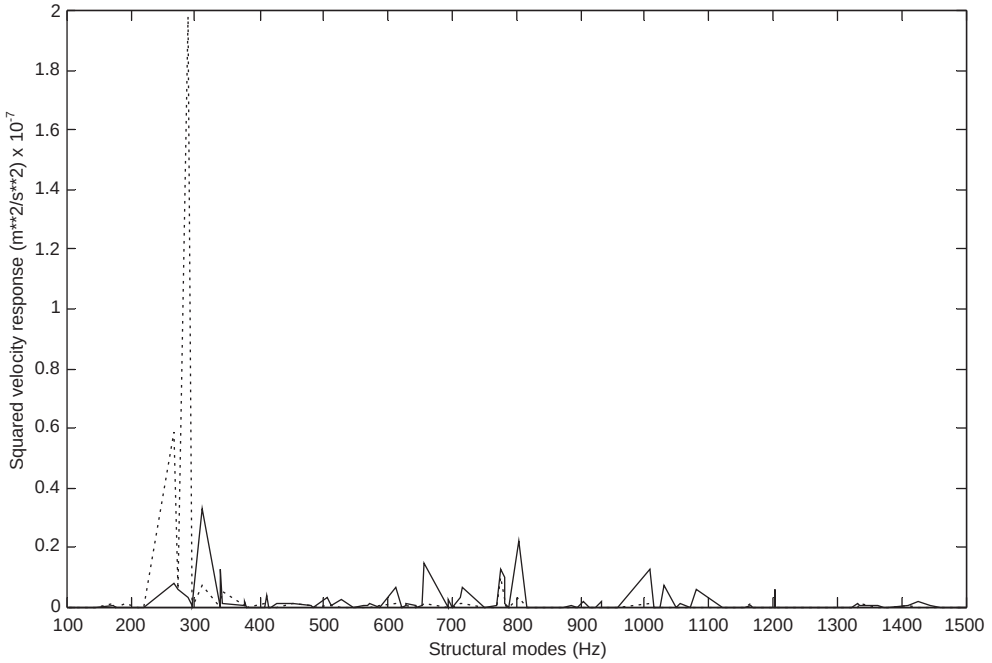

Fig. 7. Structural modal response spectrum in the case of one primary force and one control actuator (bending model): · · · · · ·: before control, ——: after control.

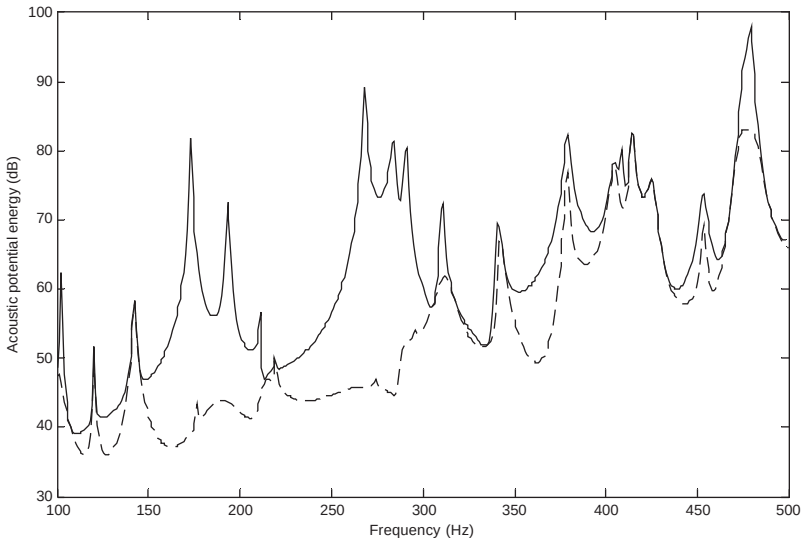

Fig. 8. Control performance of the bending model in the low-frequency range in the case of one primary force and one control actuator. ——: Before control, – – – – –: after control.

It would be interesting to verify whether the optimal configuration obtained at one particular frequency could also be effective at other frequencies. To this end, the control performance of the same control system was tested in the frequency range between 100 and 500 Hz (Fig. 8). In this figure, a significant sound reduction can be observed at most frequencies especially around 150–320 Hz. However, the sound attenuation is not achieved at a few particular frequencies. This shows that with only one control actuator operating as a bending model, the structural modes having strong sound radiation at particular frequencies cannot be effectively suppressed.

Disturbance in practice is usually more complex and multiple control PZT actuators are required. A complex case involving 10 disturbance forces with random amplitude and phase and 4 control PZT actuators is investigated. These 10 disturbance forces randomly distribute in one local area. The optimal configuration is shown in Fig. 9. In this figure, one can still observe that the optimal control actuators do not locate very close to the disturbance forces. With different disturbance force locations, the same observation is obtained. At the design frequency, the sound reduction achieved is up to 41.7 dB. The control performance in the low-frequency range (100–500 Hz) is shown in Fig. 10. One can observe that there is significant sound attenuation in the whole frequency range of interest. Peaks appearing in the uncontrolled curve correspond either to the structural resonance or acoustic resonance. After control, most peaks have been successfully eliminated. Although optimal control cannot completely eliminate all of them, they are greatly attenuated to different extent. The highest reduction is up to around 53 dB at the structural resonant frequency of 267.8 Hz. Compared with the case of one actuator, the control performance is greatly improved. This overall performance could be explained by the structural coupling analysis of the investigated structure [18], which showed that in this frequency range, the sound field is mainly contributed by a limited number of structural modes with high radiation ability. With multiple optimally designed PZT actuators, these structural modes can be effectively suppressed.

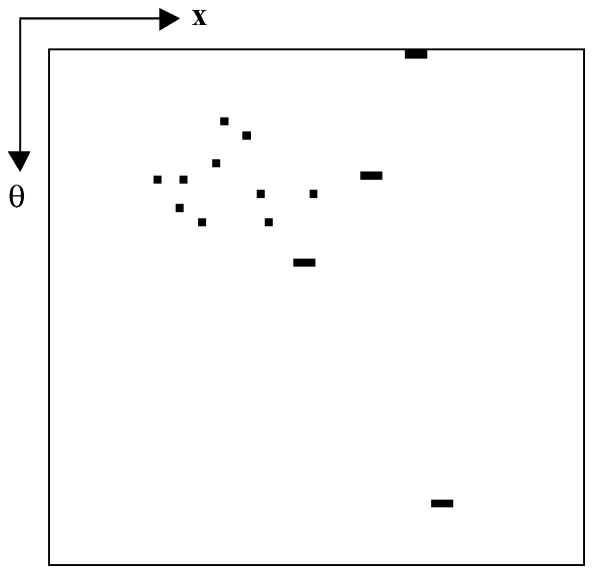

Fig. 9. Optimal placement of PZT actuators operating as a bending model in the case of ten primary forces and four control actuators. ■: Disturbance, ▬: PZT actuator.

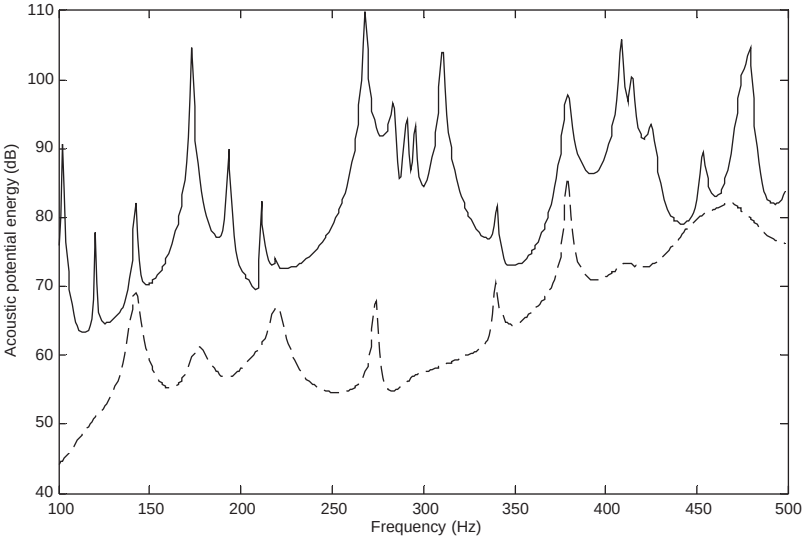

Fig. 10. Control performance of the bending model in the low-frequency range in the case of ten primary forces and four control actuators. ——: Before control, – – – –: after control.

3.3. Placement optimization of PZT actuators operating as an in-plane force model

With PZT actuators operating as an in-plane force model, the control systems are again optimized in the same two cases as in Section 3.2. Fig. 11 demonstrates the optimal configuration in the case of one disturbance force and one control PZT actuator. The optimal location of the

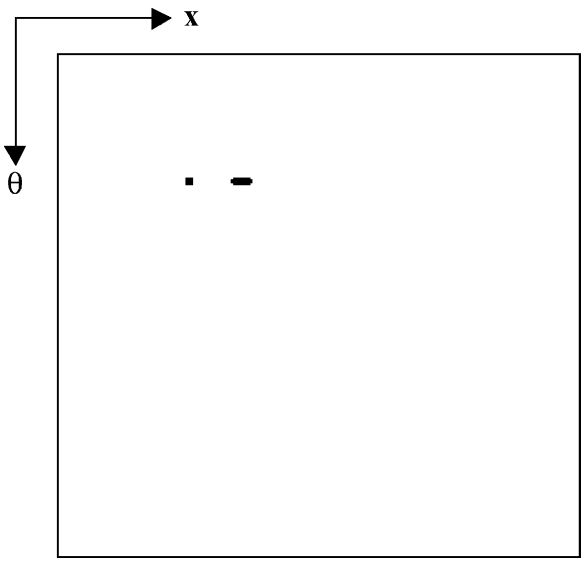

Fig. 11. Optimal placement of PZT actuators operating as an in-plane force model in the case of one primary force and one control actuator. ■ Disturbance, ▬: PZT actuator.

control actuator is (0.41, 90°). Different from the case of the bending model, the optimal position of the control PZT actuator has the same circumferential position as the disturbance. At the design frequency, the acoustic potential energy in the enclosure is reduced by 49.1 dB. The squared velocity response spectra of structural modes are shown in Fig. 12. Again, one can see that not only the two structural modes with high velocity response and strong sound radiation ability are effectively suppressed, but also every mode with perceivable response without apparent response increases at other modes. Compared with the previous bending model, the control ability on individual modes of the in-plane model seems to be much stronger.

Likewise, the control performance of the optimal configuration is tested in the low frequency range (Fig. 13). It can be observed that at all the structural and acoustic resonances in this frequency range, a sound attenuation can be achieved using the optimal configuration. Since it has the same circumferential position as the disturbance force, the control actuator can effectively act on the circumferential modes, which play an important role in radiating sound into the enclosure. A good performance in the whole low-frequency range of interest is obtained even with only one actuator.

The optimal configuration in the case of ten disturbance forces and 4 control PZT actuators is given in Fig. 14. One can see that all the four optimal actuators tend to be close to the primary sources in the circumferential direction. The investigation on many cases with different primary force locations demonstrates the same observation, which is very similar to that in the case of one disturbance and one PZT actuator. This observation is useful for one to confine the search space to a small circumferential range and hence to reduce the search time in the design. The reduction of the acoustic potential energy level at the design frequency reaches 53.6 dB. The control performance of this system in the low-frequency range below 500 Hz is shown in Fig. 15. One can see that with the optimally designed four PZT actuators operating as an in-plane force model, a significant sound reduction is achieved in the whole low-frequency range of interest even when the

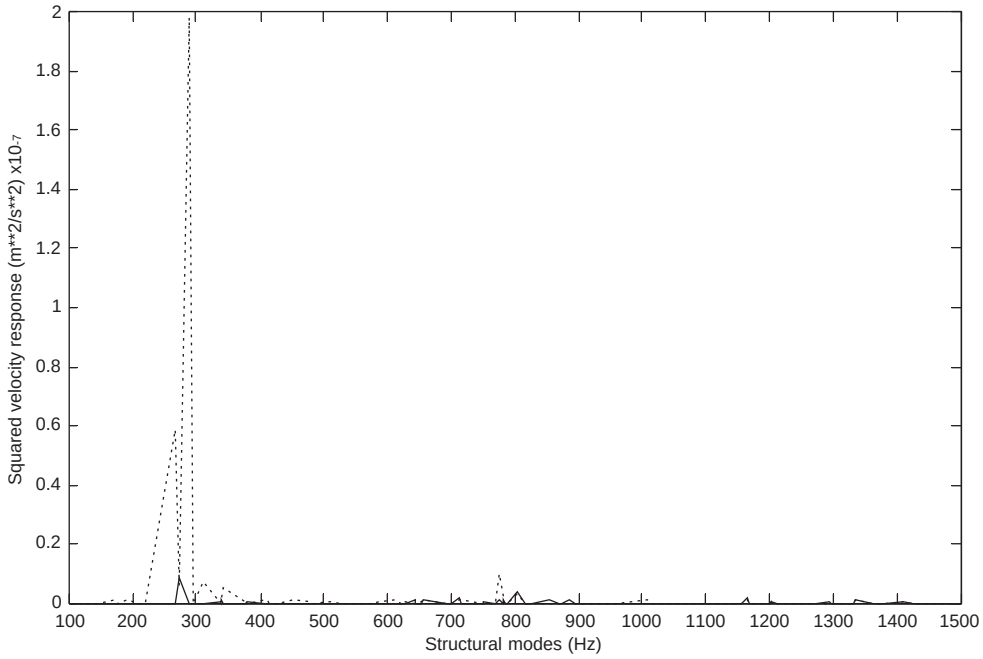

Fig. 12. Structural modal response spectrum in the case of one primary force and one control actuator (in-plane force model). · · · · ·: Before control, ——: after control.

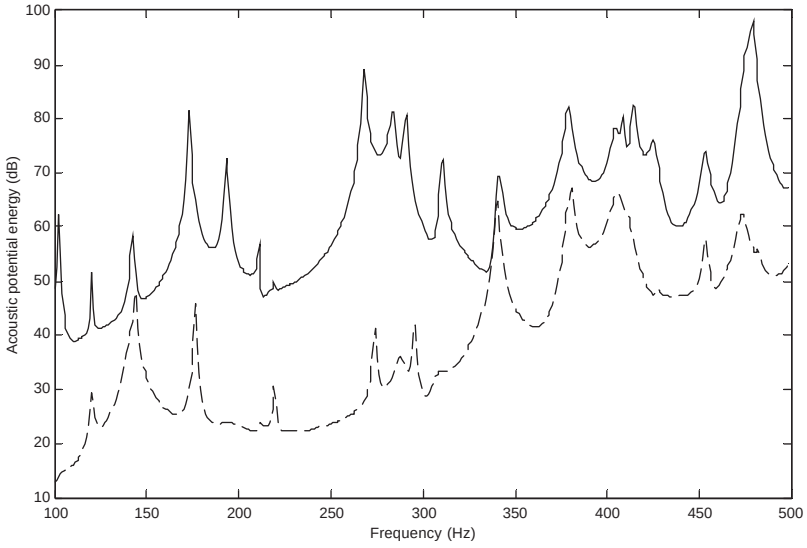

Fig. 13. Control performance of the in-plane force model in the low-frequency range in the case of one primary force and one control actuator. ——: Before control, – – – –: after control.

control actuator number is less than that of the primary forces. Most of the peaks have been eliminated. The highest reduction is up to around 64 dB at the structural resonant frequency of 267.8 Hz.

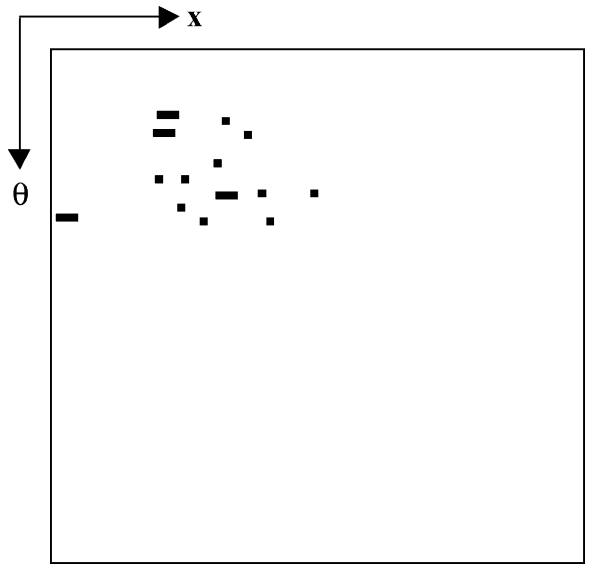

Fig. 14. Optimal placement of PZT actuators operating as an in-plane force model in the case of ten primary forces and four control actuators. ■: Disturbance, ▬: PZT actuator.

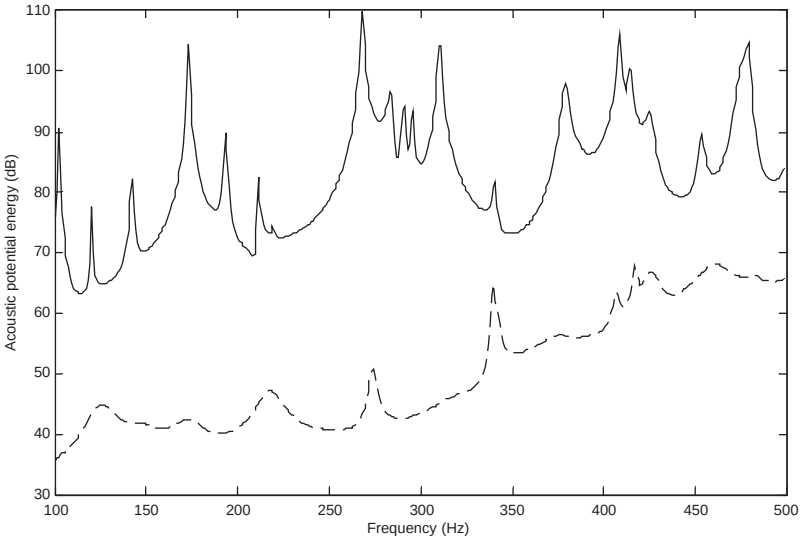

Fig. 15. Control performance of the in-plane force model in the low-frequency range in the case of ten primary forces and four control actuators. ——: Before control, – – – –: after control.

3.4. Comparison of the control performance between the bending model and the in-plane force model

The foregoing investigation demonstrates the promising performance of both the bending and the in-plane force models. It is pertinent to carry out a quantitative comparison between the two models.

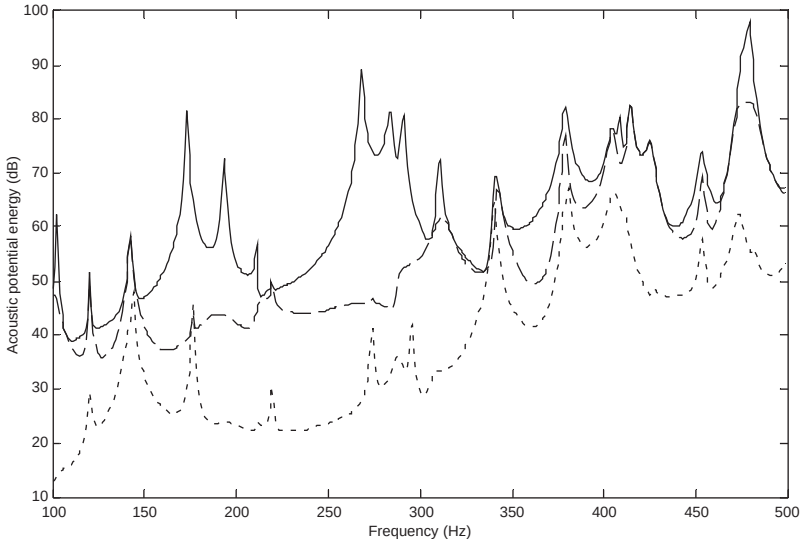

Fig. 16. Comparison of the control performance of both models in the case of one primary force and one control actuator. ——: Before control, – – – –: control with the bending model, · · · · ·: control with the in-plane force model.

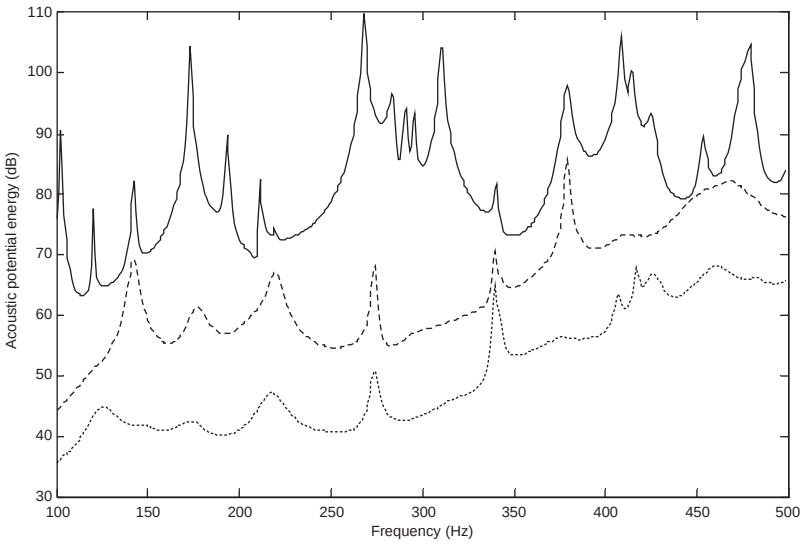

Fig. 17. Comparison of the control performance of both models in the case of ten primary forces and four control actuators. ——: Before control, – – – –: control with the bending model, · · · · ·: control with the in-plane force model.

In the case of one disturbance force and one control actuator, the comparison shows a further 12.1 dB reduction using the in-plane force model at the design frequency. Fig. 16 shows the overall performance of the two models in the low-frequency range. The in-plane force model covers a much larger area where attenuation is obtained than the bending model does. In addition, the amount of attenuation using the in-plane force model is also much higher. The same conclusion can be drawn in multi-disturbance and actuation case, as evidenced by Fig. 17, in which the

acoustic potential energies of three cases are compared (uncontrolled, bending model and in-plane force model), The increase in terms of actuators further enlarge the gap between the two models, which is typically around 15 dB. A comparison between Figs. 7 and 12 clearly illustrates the effect of these two arrangements on the modal response of the structures in the case of one disturbance and one actuator. In fact, whilst the bending model suppressing the two dominant radiating modes, the responses from some other structural modes are amplified (Fig. 7). When the in-plane force model is applied however, Fig. 12 shows a much clean suppression of almost all structural modal responses. The superiority of the in-plane model can be better understood considering the coupling between the shell and the cavity. In the low-frequency region, the membrane effect dominates the vibration of shell structures. Considering the dispersion characteristics of the shell and those of the cavity, lower-frequency modes of the shell with strong membrane effect are effectively coupled to the cavity [19]. The in-plane force model is, therefore, more capable of altering these structural modes with strong membrane effect, leading to a significant change in the coupling between the shell and the cavity.

It is pertinent to mention that other investigations (not shown) using various configurations in terms of excitation frequencies, disturbances and control configurations also support the above observations.

4. Conclusions

In this paper, the placement optimization of PZT actuators in an ASAC system for a cylindrical shell with a floor partition was investigated. Genetic algorithms were used as a research tool. To ensure an effective search performance, GA parameters (i.e., crossover probability, mutation rate, and population size) were optimally selected before the design. Two PZT actuator models were introduced. The research showed that through optimal design, a significant sound reduction could be achieved using either the bending model or the in-plane force model. While the bending model is used, the optimal location of PZTs is not necessarily close to primary forces either in the circumferential or in the longitudinal direction and there is no apparent trend. In the case of the in-plane force model however, the optimal PZT actuators tend to be confined to the primary disturbance area, especially in the circumferential direction. This observation would help confine the search space to a small circumferential range and hence reduce the search time in the design.

To increase the practical applicability of the present research, the control performance of the optimal control system was tested in the low-frequency range between 100 and 500 Hz. The results showed that for the investigated shell–floor structure, a promising sound reduction could be achieved in the whole low-frequency range of interest as well as at the design frequency using the optimally designed control system.

As far as the investigated structure is concerned, the in-plane arrangement of PZT actuators outperforms the bending one due to its stronger capability of altering structural modes, which are effectively coupled to the acoustic cavity, in the low-frequency region.

Together with PZT design, an optimal design of either acoustic or structural sensors can certainly help enhance control performance. Using distributed PVDF sensors on the structure surface to replace microphones as error sensors in an active structural acoustic control system for cavity noise problems is very useful in many practical applications where the installation of

microphones is inconvenient. The methodology proposed in the present paper can, therefore, be extended to investigate this issue. Further experimental tests are also needed to assess the whole process. Preliminary experiments in the laboratory, in which the optimally designed PZT actuators operating as the in-plane force model were used as the control sources, show very promising results. This part of the work will be reported in the future.

Acknowledgements

The work presented in this paper was supported by the Research Grants Committee of the Hong Kong SAR (Grant No. PolyU 5165/02E).

References

[1] R.L. Clark, C.R. Fuller, Optimal placement of piezoelectric actuators and polyvinylidene fluoride sensors in active structural acoustic control approaches, Journal of the Acoustical Society of America 92 (1992) 1521–1533.
[2] K.H. Baek, S.J. Elliott, Natural algorithms for choosing source locations in active control systems, Journal of Sound and Vibration 186 (2) (1995) 245–267.
[3] M.T. Simpson, C.H. Hansen, Use of genetic algorithms to optimize vibration actuator placement for active control of harmonic interior noise in a cylinder with floor structure, Noise Control Engineering Journal 44 (4) (1996) 169–184.
[4] A. Ratle, A. Berry, Use of genetic algorithms for the vibroacoustic optimization of a plate carrying point-masses, Journal of the Acoustical Society of America 104 (6) (1998) 3385–3397.
[5] S.J. Kim, K.Y. Song, Active control of sound fields from plates in flow by piezoelectric sensor/actuator, American Institute of Aeronautics and Astronautics Journal 37 (10) (1999) 1180–1186.
[6] A.J. Keane, Passive vibration control via unusual geometries: the application of genetic algorithm optimization to structural design, Journal of Sound and Vibration 185 (3) (1995) 441–453.
[7] J. Missaoui, L. Cheng, M.J. Richard, Free and forced vibration of a cylindrical shell with a floor partition, Journal of Sound and Vibration 190 (1) (1996) 21–40.
[8] L. Cheng, Vibroacoustic Modelling of Mechanically Coupled Structures: artificial spring technique applied to light and heavy medium, Shock and Vibration 3 (3) (1996) 193–200.
[9] J. Missaoui, L. Cheng, A combined integro-modal approach for prediction acoustic properties of irregular-shaped cavities, Journal of Acoustical Society of America 101 (6) (1997) 3313–3321.
[10] H.C. Lester, S. Lefebvre, Piezoelectric actuator models for active sound and vibration control of cylinder, Journal of Intelligent Material Systems and Structures 4 (1993) 295–306.
[11] R.L. Clark, C.R. Fuller, A. Wicks, Characterization of multiple piezoelectric actuators for structural excitation, Journal of Acoustical Society of America 90 (1) (1991) 346–357.
[12] E.K. Dimitriadis, C.R. Fuller, C.A. Rogers, Piezoelectric actuators for distributed vibration excitation of thin plates, Journal of Vibration and Acoustics 113 (1991) 100–107.
[13] A.W. Leissa, Vibration of shells, NASA, 1973, Sp-288.
[14] D.E. Goldberg, Genetic Algorithms in Search, Optimization and Machine Learning, Addison-Wesley, Reading, MA, 1998.
[15] Z. Michalewicz, Genetic Algorithms + Data Structures = Evolution Programs, Springer, Berlin, 1992.
[16] C.H. Hansen, S.D. Snyder, Active Control of Noise and Vibration, Spon, London, 1997.
[17] K.A. De Jong, 1975, An Analysis of the Behavior of a Class of Genetic Adaptive Systems, Doctoral dissertation, University of Michigan.
[18] D.S. Li, L. Cheng, C.M. Gosselin, Analysis of structural acoustic coupling of a cylindrical shell with an internal floor partition, Journal of Sound and Vibration 250 (5) (2002) 903–921.
[19] L. Cheng, Fluid-structural coupling of a plate-ended cylindrical shell: vibration and internal sound field, Journal of Sound and Vibration 174 (5) (1994) 641–654.